Electronic Supplementary Material (ESI) for Lab on a Chip.

A magnetically controlled microfluidic device for concentration dependent *in vitro* testing of anticancer drug

Vinit Kumar Yadav [a], Preetha Ganguly [b], Prashant Mishra [b], Samaresh Das [c], Dhiman Mallick [a]

[a] *Department of Electrical Engineering, Indian institute of technology Delhi, New Delhi, India.*

[b] *Department of Biochemical Engineering and Biotechnology, Indian institute of technology Delhi, New Delhi, India.*

[c] *The Centre for Applied Research in Electronics, Indian institute of technology Delhi, New Delhi, India.*

E-mail: dhiman.mallick@ee.iitd.ac.in

Section S1: Details on the geometrical features of the magnetically controlled microfluidic (MCM) device

The detailed structural parameters of the MCM device are illustrated in Fig. S1. The width of the microfluidic channel is 200 µm, whereas the depth of the channel is 250 µm. At a distance of 5 mm from the inlet position, the microfluidic channel is tilted at an angle of 135° (Fig. S1(a)). Further, the channel is separated into five different microchannels at a gap of 1000 µm, resulting in five corresponding outlet wells. The channel region in front of the patterned permanent magnet is called the CGG (Concentration Gradient Generation) region (Fig. S1(b)), as the concentration of the injected magnetic sample is distributed according to the magnetic field gradient generated due to the patterning of the magnet. The patterning is accomplished by adding four rectangular permanent magnets in a stair-step configuration. The first rectangular magnet is placed 150 µm from the closest channel wall, while a gap of 50 µm continuously increases as the magnet is further added, resulting in 200 µm, 250 µm, and 300 µm gaps (g) between the respective magnet and fluidic channel. Such a magnet configuration is able to create an inhomogeneous magnetic field gradient throughout the CGG region and obtain an intense field gradient peak, especially at each bifurcating junction due to the joining edges of the consecutive patterns. The diameter for the

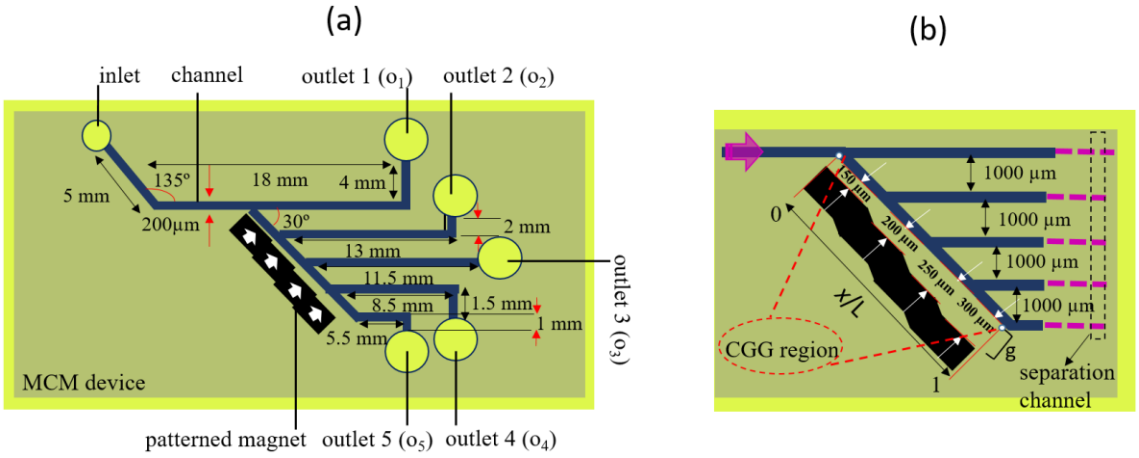

Fig. S1: Schematic representation of the MCM device (a) Design details on the magnetic microfluidic size; the depth of all channels is 250 µm. (b) Design of the patterned magnet with the CGG (concentration gradient generation) region. The white arrow inside the magnet shows the magnetization direction of the patterned magnet. The CGG region is considered for $0 < x/L < 1$ in the microfluidic channel in front of magnet arrangements.

inlet and all five outlets are 2 and 5 mm, respectively. Compared to the inlet, the outlet reservoir diameter is more significant, so a good amount of cells can be cultured comfortably.

Section S2: Details on the Numerical Simulation

Based on the device design, the simulation model is built in COMSOL Multiphysics (COMSOL 5.5). In the simulation, the magnetic field is solved using the "Magnetic field, no Current" module, the fluid flow is solved using the "Laminar Flow" module, and the particle deflection and trajectory in a non-magnetic fluid medium are solved using the "Particle Tracing for Fluid Flow" module. Table S1 shows the parameters that are used in the simulation model.

Table S1 The used parameters in the numerical simulation

Parameters	Value
Saturation magnetization	0.92 T
Density of fluid	1005.58 kg m^{-3}
Viscosity of fluid	1.059 m Pa.s
Density of particle	4800 kg m^{-3}
Diameter of particle	75 nm
Susceptibility of particle [1]	0.2

Section S3: Optimization of the flow rate to compartmentalize magnetic sample in the device

In order to compartmentalize the magnetic sample, the drag force plays a vital role in manipulating particles, as magnetic force remains constant throughout the investigation. Initially, the flow rate applicable to a separate magnetic nanoparticle, systematically, in five different separation channels, is optimized using FEM simulation in COMSOL multiphysics. Six thousand magnetic particles are injected from the inlet of the device and simulated for 100 s with a 0.1 s time interval, as shown in Fig. S2 (a). The particles at every five outlets of the channel are counted using global evaluation ('total number of particles in selection' option) after each simulation [2]. The percentage distribution of collected particles at each outlet is calculated using the following formula.

$$Collecetd\ particle\ \% = \frac{Number\ of\ partile\ at\ outlet}{Total\ Nuber\ of\ injected\ particle} \times 100$$

The particle follows uniform distribution near the inlet of the channel, whereas, in front of the patterned magnet, a concentration gradient of the particles is generated, i.e., - the CGG region. Due to the patterning of the magnet, a decaying magnetic force at each joining and end edge (x/L = 0, 0.25, 0.5, 0.75, 1) is created. However, with the increase in flow rate, the particle's hydrodynamic flow velocity $\boldsymbol{u_{hd}}$ increases linearly, as shown in Fig. S2 (b); the corresponding particle enters the separation channel and is collected at the outlets. The collected particle percentage at each outlet upon varying flow conditions in the presence of an inhomogeneous magnetic field is calculated, as shown in Fig. S2 (c-g). The result shows that if the flow velocity is low, i.e., $\boldsymbol{u_{hd}}$ < 0.19 mm s^{-1}, then most of the particle flows from the nearest wall of the channel in the CGG region due to relatively higher dominance of magnetic force over drag force, restricting the movement for outlet 1 and 2, (Fig. S2 (c, d)). In contrast, an almost similar number of particles is collected at the outlet if the flow rate is comparatively higher, i.e., $\boldsymbol{u_{hd}}$ > 0.37mm s^{-1}, as the drag force highly dominates the magnetic force, shown in Fig. S2 (g). Moreover, for the flow velocity range 0.19 mm s^{-1}< $\boldsymbol{u_{hd}}$ < 0.37 mm s^{-1}, a systematically decaying particle percentage is achieved from each outlet (Fig. S2 e, f). This is because hydrodynamic flow velocity $\boldsymbol{u_{hd}}$ is comparable in a slight increment with the magnetically induced flow velocity $\boldsymbol{u_{mg}}$, leading to no trapping and optimum particle deflection in the CGG region, leading to 100 % sample utilization. However, the drug-loaded magnetic

nanoparticle tends to agglomerate significantly higher than a nonmagnetic drug. Therefore, the device is optimized for a specific clinically acceptable, operating flow rate, i.e., 0.6 – 1.1 μL min^{-1} to compartmentalize drug samples in a wide range of concentrations of 10 - 480 μg mL^{-1}, whereas 0.85 μL min^{-1} is considered in the experiments. Moreover, particle trajectory for flow range Q = 0.05 - 2 μL min^{-1} is shown in Fig. S2 h-j using FEM simulation.

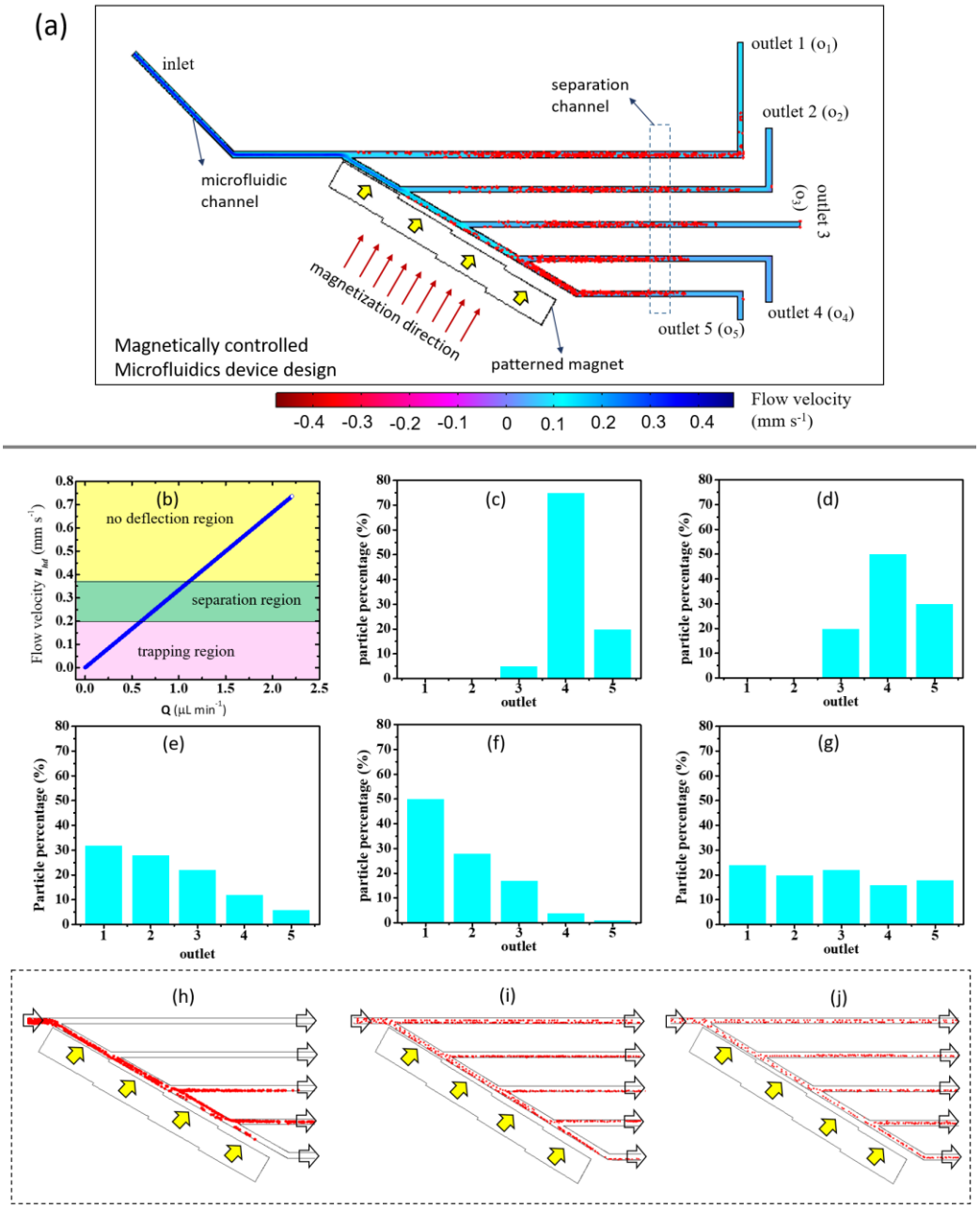

Fig. S2: (a) Particle tracing of magnetic nanoparticle injected from the inlet in a non-magnetic fluid medium at a fixed flow rate of Q = 0.85 μL min^{-1}. Particles are separated into the separation channel according to magnetic force exerted on them in the CGG region (b) Hydrodynamic flow velocity $\boldsymbol{u_{hd}}$ of the particle at various flow rates Q shows the different operating regions of the device. The calculated particle percentage at each outlet at different flow conditions (c) Q = 0.05 μL min^{-1} (d) Q = 0.25 μL min^{-1} (e) Q = 0.65 μL min^{-1} (f) Q = 0.85 μL min^{-1} (g) *Q* = 1.5 μL min^{-1}. Particle gets trapped below 0.6 μL min^{-1}. The magnetic force less affects the magnetic particle beyond 1.1 μL min^{-1}, whereas the effective flow rate for compartmentalizing particles ranges between 0.6 - 1.1 μL min^{-1}. FEM simulation of the particle trajectory in the CGG region at different flow rates Q (h) 0.05 μL min^{-1} (i) 0.65 μL min^{-1} (j) 1.5 μL min^{-1}.

Section S4: Roughness profile of the micromachined microfluidic channel

Using the optical profilometer, the surface roughness is found to be within the nanometre range (~ 50 - 200 nm), which is negligible compared to other channel geometries, such as width and depth. As a result, the fluid flow dynamics remain unaffected by this order of insignificant roughness. An optical 2D and 3D image of a particular portion of the microfluidic channel is shown in Fig. S3.

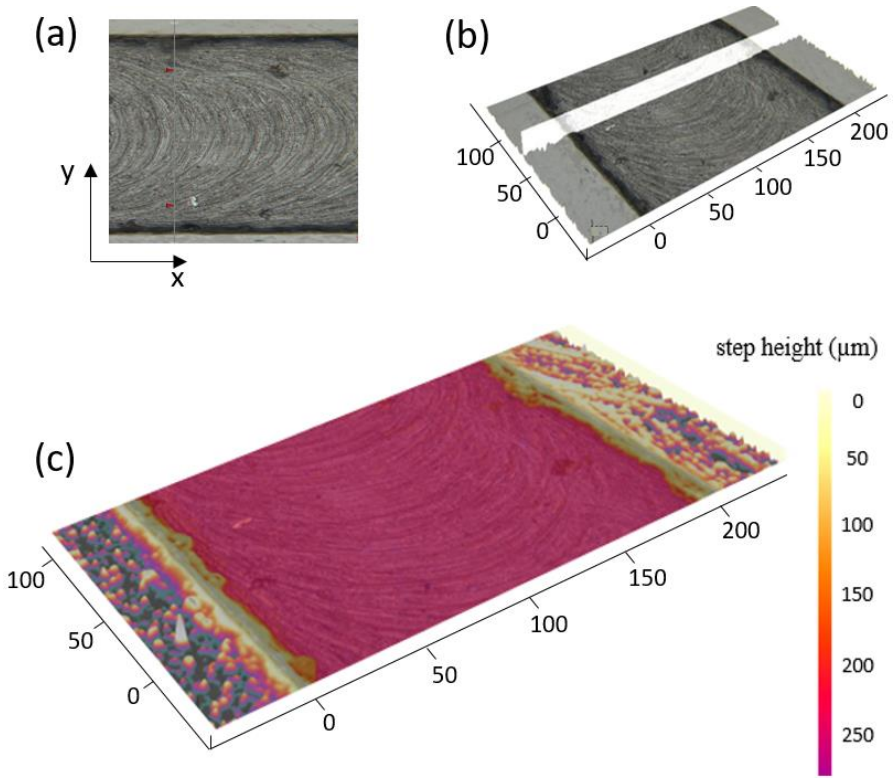

Fig. S3: Optical image of the micromachined microfluidic channel using an optical profilometer (a) 2D and (b) 3D images of a particular portion of the microfluidic channel; (c) Step height profile using color mapping.

REFERENCES

1. R. Wirix-Speetjens, W. Fyen, J. D. Boeck, G. Borghs, *Journal of Applied Physics*, 2006, 99 (10), 103903.
2. K. Y. Castillo-Torres, E. S. McLamore, and D. P. Arnold, *Micromachines*, vol. 11, no. 1, p. 16.